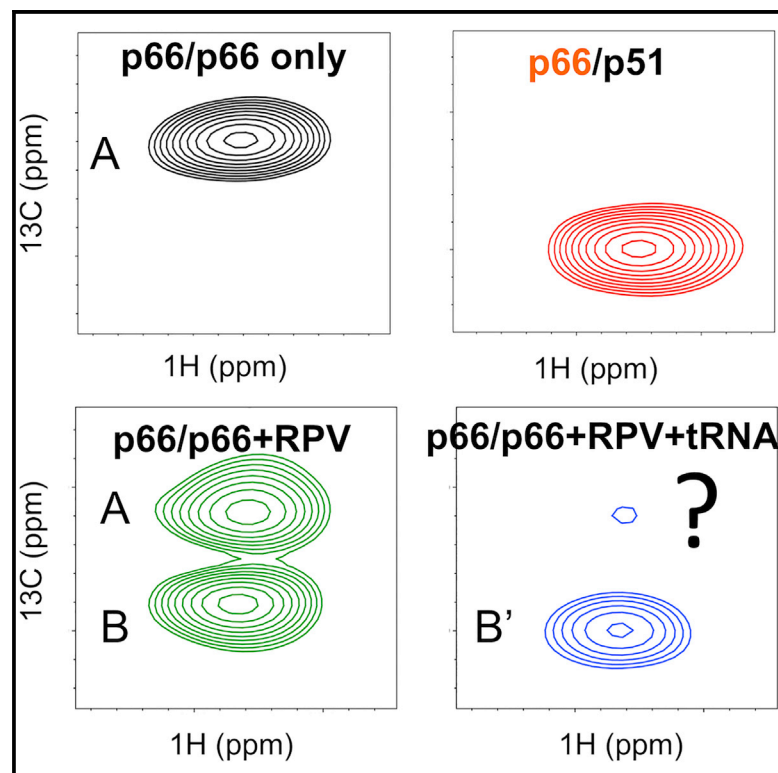


Structure

Conformational Changes in HIV-1 Reverse Transcriptase that Facilitate Its Maturation

Graphical Abstract



Authors

Ryan L. Slack, Tatiana V. Ilina, Zhaoyong Xi, ..., Stefan G. Sarafianos, Nicolas Sluis Cremer, Rieko Ishima

Correspondence

nps2@pitt.edu (N.S.C.),
ishima@pitt.edu (R.I.)

In Brief

Slack et al. characterize conformational changes involved in the maturation of HIV-1 reverse transcriptase using NMR spectroscopy. Biochemical and virological experiments are carried out to explain how these factors affect the maturation.

Highlights

- tRNA^{Lys3} mediates maturation of HIV-1 reverse transcriptase (RT) *in vitro*
- Conformational states that enhance the RT maturation were investigated using NMR
- Lys-tRNA synthetase knockdown expt suggests the tRNA^{Lys3} role in the RT maturation
- Biochemical, biophysical, and virological data support the RT maturation model

Conformational Changes in HIV-1 Reverse Transcriptase that Facilitate Its Maturation

Ryan L. Slack,¹ Tatiana V. Ilina,¹ Zhaoyong Xi,¹ Nicholas S. Giacobbi,² Gota Kawai,³ Michael A. Parniak,⁴ Stefan G. Sarafianos,⁵ Nicolas Sluis-Cremer,^{2,*} and Rieko Ishima^{1,6,*}

¹Department of Structural Biology, University of Pittsburgh School of Medicine, Room 1037, Biomedical Science Tower 3, 3501 Fifth Avenue, Pittsburgh, PA 15260, USA

²Department of Medicine, Division of Infectious Diseases, University of Pittsburgh School of Medicine, Pittsburgh, PA 15261, USA

³Department of Life and Environmental Sciences, Chiba Institute of Technology, Chiba, Japan

⁴Department of Microbiology and Molecular Genetics, University of Pittsburgh School of Medicine, Pittsburgh, PA 15219, USA

⁵Laboratory of Biochemical Pharmacology, Department of Pediatrics, Emory University School of Medicine, Atlanta, GA 30322, USA

⁶Lead Contact

*Correspondence: nps2@pitt.edu (N.S.C.), ishima@pitt.edu (R.I.)

<https://doi.org/10.1016/j.str.2019.08.004>

SUMMARY

HIV-1 reverse transcriptase (RT) is translated as part of the Gag-Pol polyprotein that is proteolytically processed by HIV-1 protease (PR) to finally become a mature heterodimer, composed of a p66 and a p66-derived 51-kDa subunit, p51. Our previous work suggested that tRNA^{Lys3} binding to p66/p66 introduces conformational changes in the ribonuclease (RNH) domain of RT that facilitate efficient cleavage of p66 to p51 by PR. In this study, we characterized the conformational changes in the RNH domain of p66/p66 imparted by tRNA^{Lys3} using NMR. Moreover, the importance of tRNA^{Lys3} in RT maturation was confirmed *in cellulo* by modulating the levels of Lys-tRNA synthetase, which affects recruitment of tRNA^{Lys3} to the virus. We also employed nonnucleoside RT inhibitors, to modulate the p66 dimer-monomer equilibrium and monitor the resulting structural changes. Taken together, our data provide unique insights into the conformational changes in p66/p66 that drive PR cleavage.

INTRODUCTION

Efficient maturation of HIV-1 proteins is critical for virus replication. HIV-1 reverse transcriptase (RT) is expressed as part of the viral Gag-Pol polyprotein, which is cleaved by HIV-1 protease (PR) to finally form a mature RT heterodimer composed of 66-kDa (p66) and 51-kDa (p51) subunits (p66/p51) (Figure 1A) (Coffin et al., 1997; Katz and Skalka, 1994). The p51 subunit is generated upon removal of most of the ribonuclease H (RNH) domain from p66 (Chattopadhyay et al., 1992; Divita et al., 1995; Sharma et al., 1994). Two models of RT maturation have been proposed: a *concerted* model, in which the p66 and p51 subunits are cleaved independently from Gag-Pol, and a *sequential* model, in which PR first cleaves p66 from the polyprotein and, following p66 dimerization, the p66/p51 RT heterodimer

is formed (Figueiredo et al., 2006; Lindhofer et al., 1995; Mattei et al., 2014; Pettit et al., 2004, 2005b; Sluis-Cremer et al., 2004; Speck et al., 2000; Wapling et al., 2005; Zheng et al., 2014, 2015). Regarding these models, previous biochemical data, including ours, demonstrated that p66/p66 homodimer formation is absolutely necessary for efficient *in vitro* RT maturation, thus supporting the sequential model (Figure 1C) (Abram and Parniak, 2005; Abram et al., 2010; Sluis-Cremer et al., 2004). Paradoxically, the p66/p66 homodimer adopts a symmetrical conformation in solution in which both RNH domains are folded and the p51-RNH cleavage sites are inaccessible to PR (Sharaf et al., 2014). Interestingly, in all structures of the mature p66/p51 heterodimer, the p51-RNH cleavage site is sequestered in a β sheet within the RNH domain and is inaccessible to PR (Figure 1B) (Davies et al., 1991; Jacobo-Molina and Arnold, 1991; Jacobo-Molina et al., 1993; Kohlstaedt et al., 1992). Consequently, the pathways involved in p66/p51 RT maturation have not been defined. However, characteristic differences between the immature p66/p66 homodimer and the mature p66/p51 heterodimer, such as a ~ 10 -fold decrease in the dimer dissociation constant (Sharaf et al., 2014; Sluis-Cremer et al., 2000; Venezia et al., 2006), have led to the hypothesis that significant structural differences exist between these RT proteins.

Recently, we developed an *in vitro* RT maturation assay that evaluates processing of p66 by active HIV-1 PR to yield p66/p51 heterodimer, and we proposed that interaction of tRNA^{Lys3} with the p66/p66 homodimer enhances specific cleavage by PR at the p51-RNH cleavage site (Ilina et al., 2018). Although this study identified key factors in RT maturation including: (1) the fundamental importance of homodimer formation; (2) an interaction between tRNA^{Lys3} and p66/p66; and (3) enhancement of p66/p51 production in the presence of tRNA^{Lys3}, the *conformational changes* that the p66/p66 homodimer undergoes during maturation are unknown. Another detail of the sequential model that remained unclear was whether tRNA^{Lys3} enhanced p66/p51 production due to its ability to increase p66/p66 homodimer formation, or if a specific p66/p66 conformation induced by tRNA^{Lys3} was required for the RT maturation. Although tRNA, especially tRNA^{Lys3}, is abundantly present in the virus (Jiang et al., 1992, 1993; Kleiman et al., 1991; Mak et al., 1994; Pavon-Eterod et al.,

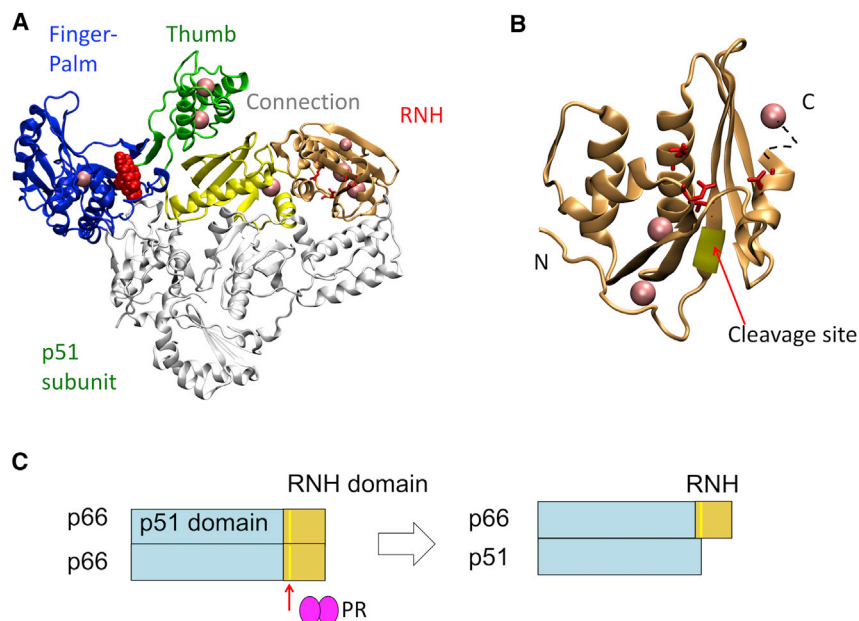


Figure 1. Structure of p66/p51 HIV-1 RT

(A) Overall structure of the p66/p51 heterodimer. The fingers-palm, thumb, connection, and RNH domains in the p66 subunit are purple, green, yellow, and orange, respectively. The p51 subunit is white.

(B) Structure of the RNH domain highlighting that the p51-RNH cleavage site (F440-Y441, yellow ribbon) is sequestered in the protein core. The RNH active site residues are shown by red sticks.

(C) Schematic highlighting how p66/p51 is generated from p66/p66 by HIV-1 PR-mediated cleavage. In (A and B), graphics were generated using the structure of PDB: 3MEE (Lansdon et al., 2010); the location of RPV is shown by red spheres in (A); locations of the Ile- δ 1 methyl groups that were uniquely observed in the NMR data are shown by pink spheres. These are residues 202 in the fingers-palm domain, 254 and 259 in the thumb domain, 393 in the connection domain, and 434, 495, and 559 in the RNH domain. Note, because crystallographic coordinates are not available for residue 559, the position of residue 559 is approximated.

2010), it is also unclear whether tRNA^{Lys3} affects RT maturation in the virus to impact viral replication.

Herein, we present an analysis of the conformational changes of p66/p66 homodimer upon tRNA^{Lys3} interaction in solution, as well as changes in PR-mediated production of p66/p51, using NMR spectroscopy. Since our previous data suggested that p66 undergoes fast monomer-dimer equilibrium (Sharaf et al., 2014), and that tRNA^{Lys3} interacts with p66 monomer as well as the p66/p66 homodimer (Iliina et al., 2018), we designed experiments to distinguish the homodimer interaction with tRNA^{Lys3} from that of the monomer. We achieved this by using non-nucleoside reverse transcriptase inhibitors (NNRTIs) known to interact with the p66/p66 homodimer at a 1:1 stoichiometry, to enhance p66/p66 homodimer formation, and to change the environment of the NNRTI binding pocket in p66/p66 similar to that of the p66/p51 (Braz et al., 2010; Sharaf et al., 2017; Tachedjian et al., 2005). Importantly, using *in vitro* RT maturation experiments and by employing size exclusion chromatography (SEC) of the protein in various conditions, we show that the application of NNRTIs alone does not alter our underlying premise that tRNA^{Lys3} binding to p66/p66 generates a conformational change in the homodimer that facilitates RT maturation. Notably, in HIV-1, the primer tRNA, tRNA^{Lys3}, is required for reverse transcription initiation complex formation, and is recruited to the virus by interacting with lysine-tRNA synthetase (KARS) (Cen et al., 2001, 2002; Khorchid et al., 2000; Kleiman and Cen, 2004; Kleiman et al., 2010; Mak et al., 1994, 1997). Therefore, we also assessed the impact of tRNA^{Lys3} on RT maturation by KARS knockdown in HIV-1 producing cells.

RESULTS

NMR Spectra of p66/p66 Homodimer

To gain insight into the conformational changes in p66/p66 that facilitate *in vitro* RT maturation, we monitored the ¹H-¹³C HMQC spectral features of [U-²H], Ile δ 1-[¹³CH₃]p66 protein over time in

solution at 35°C (Figures 2A and 2B). As described in the STAR Methods, we used four columns to purify p66 for NMR, to avoid contamination by *E. coli* proteases that can process p66 to p51 (Bavand et al., 1993; Clark et al., 1995; Lowe et al., 1988). These experiments were performed using a concentration of 35 μ M (as p66/p66), a concentration at which we would expect 80% of the protein to exist as a homodimer. The overall HMQC spectral features of the protein did not change over 50 h (Figure S1), consistent with our previous observation using ¹H-¹⁵N NMR of [U-²H, ¹⁵N]p66 (Sharaf et al., 2014). A small reduction in the NMR signal intensity (~15%) was observed, presumably due to instability of the magnet or protein solution (Figure 2C); a gain in signal intensity would be expected if protein unfolding occurred. The spectrum shows a set of protein resonances that are indicative of a symmetric homodimeric form of p66/p66, consistent with previously published p66/p66 spectra, albeit lacking evidence of previously described slow conformational changes that had occurred over 40 h (Zheng et al., 2014, 2015, 2017). In addition, as previously observed, several resonances overlapped in the central region of the spectrum (dashed rectangular in Figure 2A) even though the Ile δ 1-methyl-labeled residues are distributed across the p66 domains (highlighted by pink spheres in Figure 1A) (Zheng et al., 2014, 2015, 2017).

The observed spectral features of p66/p66 homodimer were compared with those of the p66/p51 heterodimer (Figure 2D) and with a partially matured sample in which p66/p66 was incubated with HIV-1 PR in the presence of tRNA^{Lys3} (Figure 2E). Consistent with previously published data (Zheng et al., 2014), the p66/p66 NMR spectrum was distinct compared with that of p66/p51. When PR was added to p66/p66 in the presence of tRNA^{Lys3}, we observed an increase in the signal intensity at the random coil position (Figure 2F) and a spectral pattern similar to that of p66/p51 (Figure 2E). Because the cleavage of p66/p66 to p66/p51 was incomplete, spectral patterns for both p66/p66 and p66/p51 can be observed in Figure 2E. Overall, the observed spectral features of p66/p66 are distinct compared with those

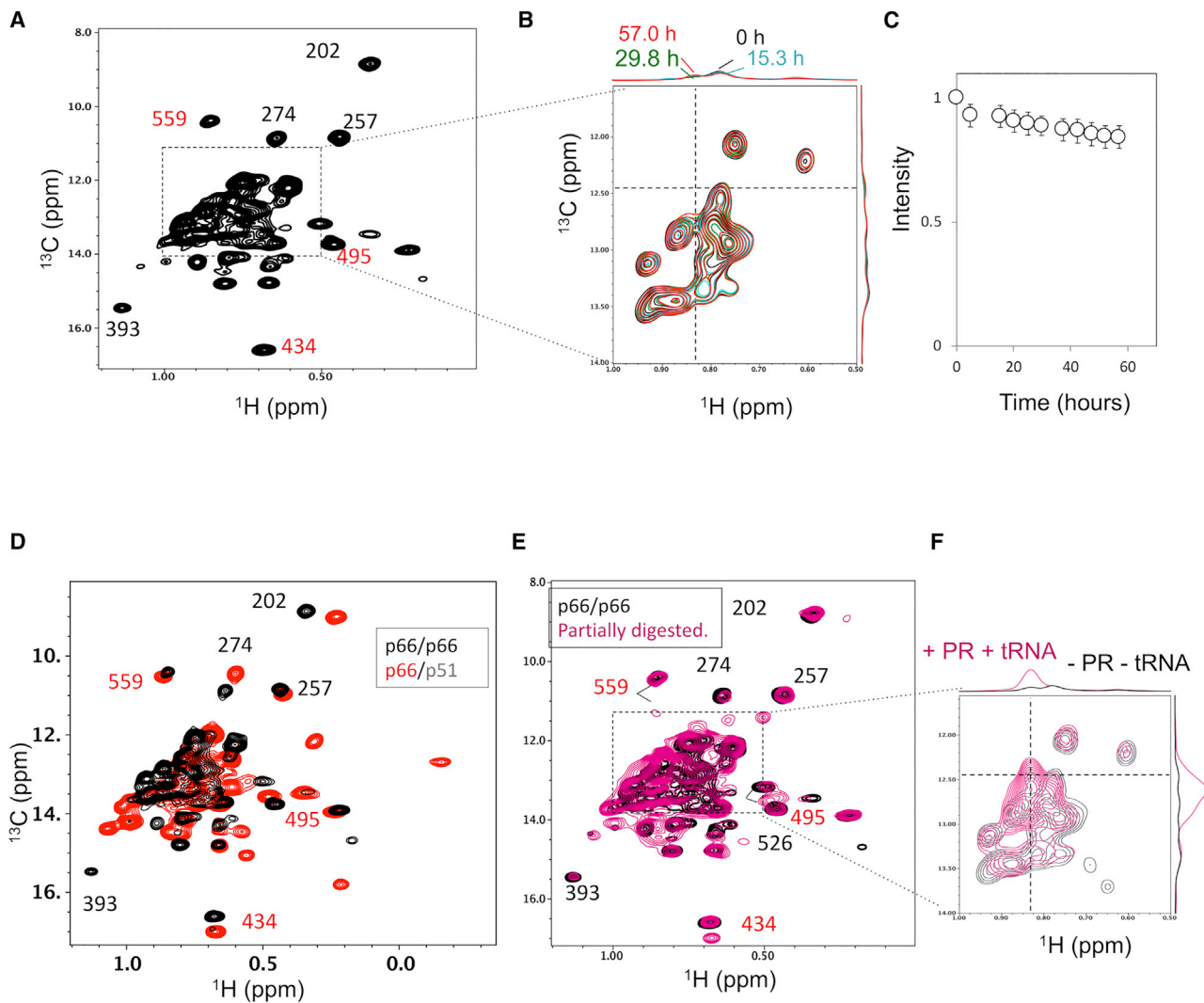


Figure 2. ^1H - ^{13}C SOFAST TROSY-HMQC NMR Spectra of $[\text{U}\text{-}^2\text{H}]$, Ile $\delta 1$ - $^{13}\text{CH}_3$]p66/p66 at 35°C

(A) p66/p66 spectrum immediately following NMR sample preparation; (B) the random coil region of the spectrum shown in (A) is overlaid with NMR spectra obtained for the same sample at 2.9, 25, and 57 h; (C) a plot of the average intensity decay of 42 resonances collected from p66/p66 over 57 h; (D) comparison of the p66/p66 spectrum (black) with that of a p66/p51 sample (red) in which only the p66 subunit was labeled with $[\text{U}\text{-}^2\text{H}]$, Ile $\delta 1$ - $^{13}\text{CH}_3$; (E) comparison of the p66/p66 spectrum (black) with that after 3 h digestion of the NMR sample by active PR in the presence of unlabeled tRNA^{Lys3} (pink, see the STAR Methods); (F) the indicated area of the spectrum in (E) is shown at high threshold level. Residue numbers (those in the RNH domain are colored red), except for I559, were based on previous literature (Zheng et al., 2014). In (B and F), slices taken at the dashed lines, in which cross-section, ^1H 0.83 ppm and ^{13}C 12.6 ppm, is nearly at the random coil position of the Ile- $\delta 1$ methyl group (Wishart et al., 1995), are plotted along the outer edge of the spectrum. Note, since approximately 80% of the p66 forms a homodimer at the p66 concentration used in this study, we use the notation of p66/p66, to compare with the p66/p51. See also Figure S1.

of p66/p51 and are suggestive of a symmetric homodimer conformation.

NMR Spectra of p66 in the Presence of tRNA^{Lys3}

We hypothesized that tRNA^{Lys3} interaction with p66/p66 introduces conformational changes in a single RNH domain that facilitate efficient cleavage of p66 to p51 by HIV-1 PR (Iliina et al., 2018). To address the hypothesis, we monitored changes in the ^1H - ^{13}C HMQC spectrum of $[\text{U}\text{-}^2\text{H}]$, Ile $\delta 1$ - $^{13}\text{CH}_3$]p66 protein in the absence and presence of unlabeled tRNA^{Lys3} at a [tRNA^{Lys3}]:[p66/p66] = 1.4:1 molar ratio. We observed that upon addition of tRNA^{Lys3}, the p66 spectrum, which shows

only p66 signals and not tRNA^{Lys3}, exhibited a slight increase in the signal intensity, nearly at the random coil position of the Ile- $\delta 1$ methyl group at ^1H 0.83 ppm and ^{13}C 12.6 ppm (Wishart et al., 1995) (cross-section of the dashed lines in Figure 3A), suggesting partial unfolding of the protein, although many of the resonance positions did not change (Figure 3A, discussed below).

Because methyl signal intensities, as peak height, are mainly determined by a fast methyl three-site jump (Nicholson et al., 2002), Ile $\delta 1$ -methyl ^1H - ^{13}C spectra are less sensitive to reductions in domain motion compared with backbone ^1H - ^{15}N amide NMR spectra, which are more sensitive to changes in molecular

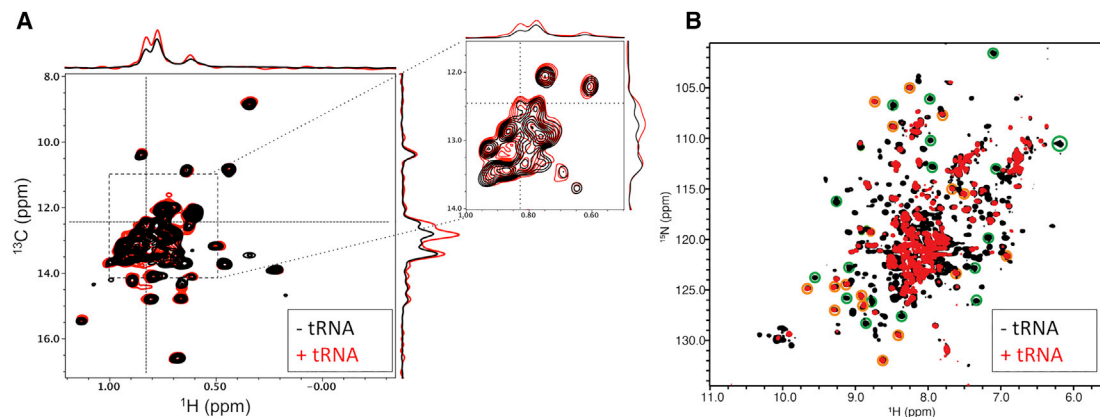


Figure 3. NMR Spectra of p66 in the Presence of tRNA^{Lys3}

(A) ^1H - ^{13}C SOFAST-HMQC NMR spectra of $[\text{U-}^2\text{H}, ^{15}\text{N}]\text{p66/p66}$ recorded at 35°C and (B) ^1H - ^{15}N TROSY-HSQC NMR spectra of $[\text{U-}^2\text{H}, ^{15}\text{N}]\text{p66/p66}$, in the absence (black) or presence (red) of unlabeled tRNA^{Lys3}, recorded at 20°C . In (A), a selected region (box) is shown at high threshold level with slices taken at the dashed lines, the cross-section of which is nearly at the random coil position. In (B), resonances that were previously found to overlap with the isolated thumb and RNH domains are circled by green and orange colors, respectively (Sharaf et al., 2014). Note, a lower temperature was used for the ^1H - ^{15}N experiments compared with the temperature used for the ^1H - ^{13}C experiments, presuming greater protein stability at a lower temperature.

tumbling, domain motion, and internal motion. To further elucidate the conformational changes of p66/p66 imparted by tRNA^{Lys3} binding, we also recorded ^1H - ^{15}N TROSY-HSQC spectra of $[\text{U-}^2\text{H}, ^{15}\text{N}]\text{p66}$ in the absence and presence of tRNA^{Lys3} at a $[\text{tRNA}^{\text{Lys3}}]:[\text{p66/p66}] = 1:1$ molar ratio (Figure 3B). At $75\ \mu\text{M}$, p66/p66 contains $\sim 90\%$ dimer, with fast exchange occurring between monomer and dimer. The ^1H - ^{15}N TROSY-HSQC spectrum exhibits a single set of clearly identifiable signals stemming from the RNH and thumb domains (circled orange and green, respectively, in Figure 3B) based on previous assignments, suggesting symmetrical p66/p66 conformation in solution (Sharaf et al., 2014). As reported previously (Sharaf et al., 2014), the resonance positions of the thumb and RNH domains within p66 spectra were highly similar to those of the isolated domains, and also to those in p51. Reported dissociation constants indicate that the p66 homodimer has a 10-fold higher affinity than that of the p51 homodimer at equilibrium (Sharaf et al., 2014; Venezia et al., 2006). Based on these observations, and the assumption that resonances observed for the p66 dimer/monomer equilibrium were in the fast exchange regime, we derived a model in which the thumb and RNH domains undergo domain motion, allowing for the observed resonance similarity with respect to spectra of the isolated domains (Sharaf et al., 2014). Indeed, the observation of one set of resonances in the Ile $\delta 1$ -methyl ^1H - ^{13}C spectra is consistent with the ^1H - ^{15}N data (Figure 3).

Upon tRNA^{Lys3} addition, many resonances in the ^1H - ^{15}N NMR spectrum of p66/p66 exhibited a significant reduction in intensity. In particular, signals from the thumb domain significantly decreased, undergoing line broadening or disappearance upon interaction with tRNA^{Lys3}, while resonances from the RNH domain remained mostly unchanged. This reduction in the signal intensity of the thumb domain resonances is reasonable in the sense that nucleic acid binding would reduce the domain motion of the thumb, resulting in a decrease in signal intensities. It is also consistent with existing structural data, which clearly show that the canonical nucleic acid binding site in RT involves extensive

contacts with the p66 thumb and fingers-palm subdomains (Bakhanashvili and Hizi, 1994; Jacobo-Molina et al., 1993). On the other hand, if the RNH domain were in an equilibrium between either rigid and mobile domain states or folded and unfolded states, then the signals would be expected to broaden as a result of the exchange equilibrium. Thus, our observation of the RNH resonances may signify that one RNH domain remains mobile in the tRNA^{Lys3}-bound form of p66/p66 (discussed below).

NNRTI Minimizes p66 Monomer Interaction with tRNA^{Lys3}

As previously mentioned, the p66/p66 sample contains both monomer and dimer species in equilibrium. Because NMR resonance intensities are inversely proportional to the hydrodynamic radius of macromolecules in solution, even small amounts of monomer-bound tRNA^{Lys3} could potentially complicate our interpretation of NMR data. NNRTIs have been shown to promote homodimerization of the polyprotein Pol and p66 in cells and *in vitro* (Braz et al., 2010; Sharaf et al., 2017; Tachedjian et al., 2005). We therefore hypothesized that the inclusion of an NNRTI could be used to reduce the monomeric p66 species within our NMR sample. To confirm that NNRTIs are useful to reduce the monomer component of our p66/p66 samples, we first performed analytical SEC experiments with p66 in the absence or presence of NNRTI and/or tRNA^{Lys3}. As previously reported, the SEC elution profile of p66 protein alone showed both monomer and dimer elution peaks with a UV254/UV280 ratio of ~ 0.5 , while the SEC profile of tRNA^{Lys3}, also monitored by fluorescence, showed a single elution peak with a UV254/UV280 ratio of ~ 2 (Figures 4A and 4B). In the presence of a small amount of tRNA^{Lys3} ($[\text{p66/p66}]:[\text{tRNA}^{\text{Lys3}}] = 1:0.22$ molar ratio), the elution peak of the dimer shifted to a larger molecular mass, presumably a tRNA-bound form (Figure 4C). However, with excess tRNA^{Lys3} ($[\text{p66/p66}]:[\text{tRNA}^{\text{Lys3}}] = 1:1.25$), a new elution peak, located between the monomer and dimer peaks and presumably tRNA-bound p66 monomer, appeared (Figure 4D). Indeed, as described previously, even in the presence of a small amount

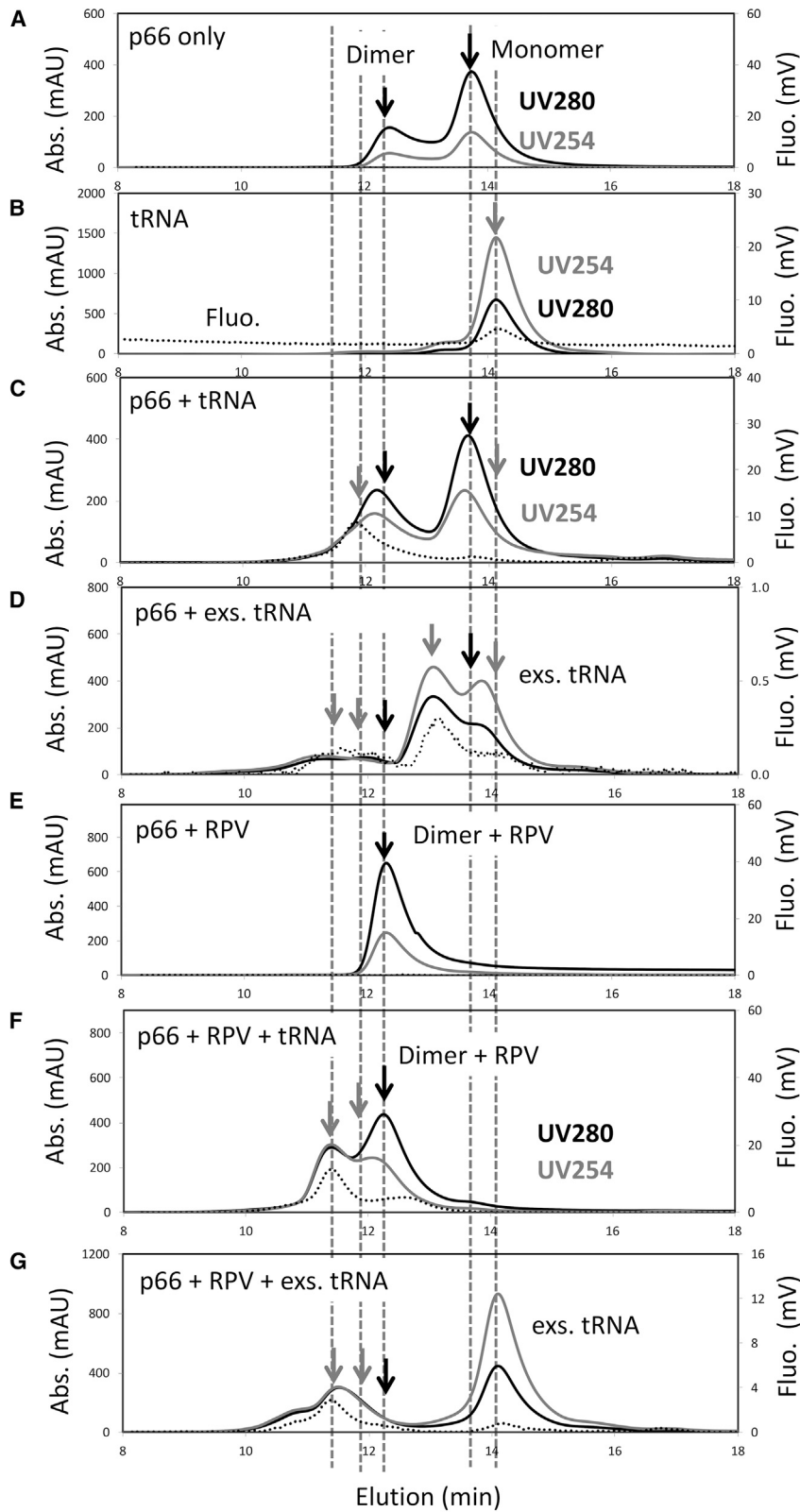


Figure 4. SEC Elution Profiles of p66

(A) p66 only, (B) tRNA^{Lys3} only, (C) p66 and tRNA^{Lys3} at [p66/p66]:[tRNA^{Lys3}] = 1:0.22, (D) p66 and tRNA^{Lys3} at [p66/p66]:[tRNA^{Lys3}] = 1:1.25, (E) p66 and RPV at [p66:p66]:[RPV] = 1:1.3 ratio, (F) p66, RPV, and tRNA^{Lys3} at [p66/p66]:[RPV]:[tRNA^{Lys3}] = 1:1.3:0.22, and (G) p66, RPV, and tRNA^{Lys3} at [p66/p66]:[RPV]:[tRNA^{Lys3}] = 1:1.5:2.0. Elution profiles were monitored by UV absorbance at 280 nm (black line) and 254 nm (gray line), and by fluorescence detection for the labeled tRNA^{Lys3} (dotted line). Black and gray arrows indicate protein alone elution peaks and those containing tRNA^{Lys3}, respectively. Note, the molar extinction coefficient of tRNA^{Lys3} at 254 and 280 nm are 10.2 and 1.8 times those of p66, respectively, and in (D) the elution peaks of free tRNA^{Lys3} and monomer p66 partially overlap with that of the tRNA^{Lys3}-bound monomer p66, which we estimate to be 20%–40% of total p66.

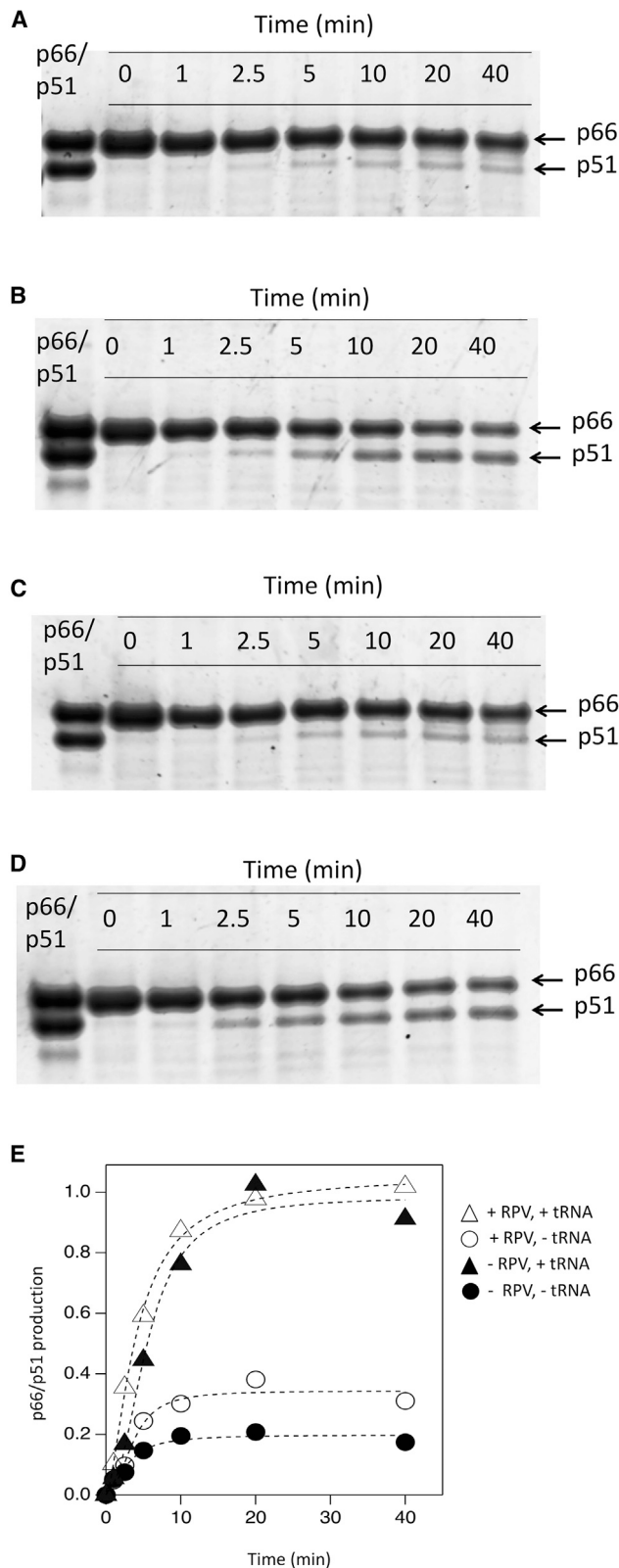


Figure 5. Time-dependent Proteolytic Cleavage of p66 by HIV-1 PR Monitored by SDS-PAGE

Cleavage experiments were conducted in the absence (A and B) or presence (C and D) of RPV, and presence (B and D) or absence (A and C) of tRNA^{Lys3}. In

of tRNA^{Lys3} (Figure 4C), the maximum position of the p66 monomer at UV254 slightly shifted from that of UV280, suggesting the existence of a tRNA^{Lys3}-p66 monomer-bound form, the retention of which may depend on the rate of exchange between the monomer and dimer fractions, or of the complexes.

The NNRTI rilpivirine (RPV) is known to enhance p66 homodimer formation with an apparent RPV-p66/p66 dissociation constant of $0.86 \pm 0.064 \mu\text{M}$ (Braz et al., 2010; Hughes, 2001; Sharaf et al., 2017; Tachedjian et al., 2001, 2005; Venezia et al., 2006). Thus, not surprisingly, in the presence of RPV, the SEC profile of p66/p66 exhibited only a homodimer fraction, and a monomer elution peak was not detected (Figure 4E). RPV is known to bind to p66/p66 with a 1:1 ratio (Sharaf et al., 2016, 2017). Incubation of RPV-bound p66/p66 with a small amount of tRNA^{Lys3} did not produce the tRNA^{Lys3}-p66 monomer peak that was seen in the absence of RPV, but, instead, produced a single elution peak, earlier than the p66/p66 homodimer, which is presumably tRNA^{Lys3}-bound p66/p66 and may include its oligomer in an exchange equilibrium (Figure 4F). Even with 2-fold excess tRNA^{Lys3}, the tRNA^{Lys3}-bound p66 monomer form was not observed in the presence of RPV (Figure 4G).

Effect of NNRTIs on the Maturation of HIV-1 RT *In Vitro*

Our SEC data clearly indicate that an NNRTI can suppress the amount of p66 monomers in our p66/p66 samples. To further characterize how NNRTI-mediated reduction in the p66 monomer component modulates RT maturation, we conducted *in vitro* RT maturation assays. In these experiments, purified p66 is incubated with HIV-1 PR and the cleavage of p66 to p51 is monitored by SDS-PAGE (Iliina et al., 2018), and generation of equivalent amounts of p66 and p51 is indicative of p66/p51 heterodimer production. Incubation of p66 alone with PR does not result in significant p66/p51 heterodimer formation (Figure 5A), whereas addition of tRNA^{Lys3} does (Figure 5B) (Iliina et al., 2018). Of note, in the absence of NNRTI, p66 exists in monomer-dimer equilibrium with a 4–10 μM dissociation constant for the homodimer (Sharaf et al., 2014; Sluis-Cremer et al., 2000; Venezia et al., 2006), similar to the concentration of p66 used in these experiments (4 μM as p66/p66). Previously, we have also shown that heterodimer production is more efficient at higher protein concentration, i.e., homodimer formation is necessary (Iliina et al., 2018).

When the monomer component of the p66 sample was suppressed by addition of 4 μM RPV (a similar molar ratio was used for the SEC experiments), we found that PR-mediated processing of p66 was mostly unchanged (Figures 5C and S2). Neither varying the RPV concentration (Figure S3), nor using efavirenz, which belongs to a different NNRTI class (Figure S4), altered the p66 processing kinetics. In contrast, addition of tRNA^{Lys3} to p66/p66 in the presence of RPV promoted efficient RT maturation, which was similar to that observed in the presence of tRNA^{Lys3} alone (Figures 5D and 5E). Collectively, these

(E), p51 band intensities shown in (A–D) were quantified and plotted. Concentrations of p66 and PR were 4 μM , as p66/p66 homodimer, and 1 μM , respectively. Both tRNA^{Lys3} and RPV concentrations were 4 μM . See also Figures S2–S4.

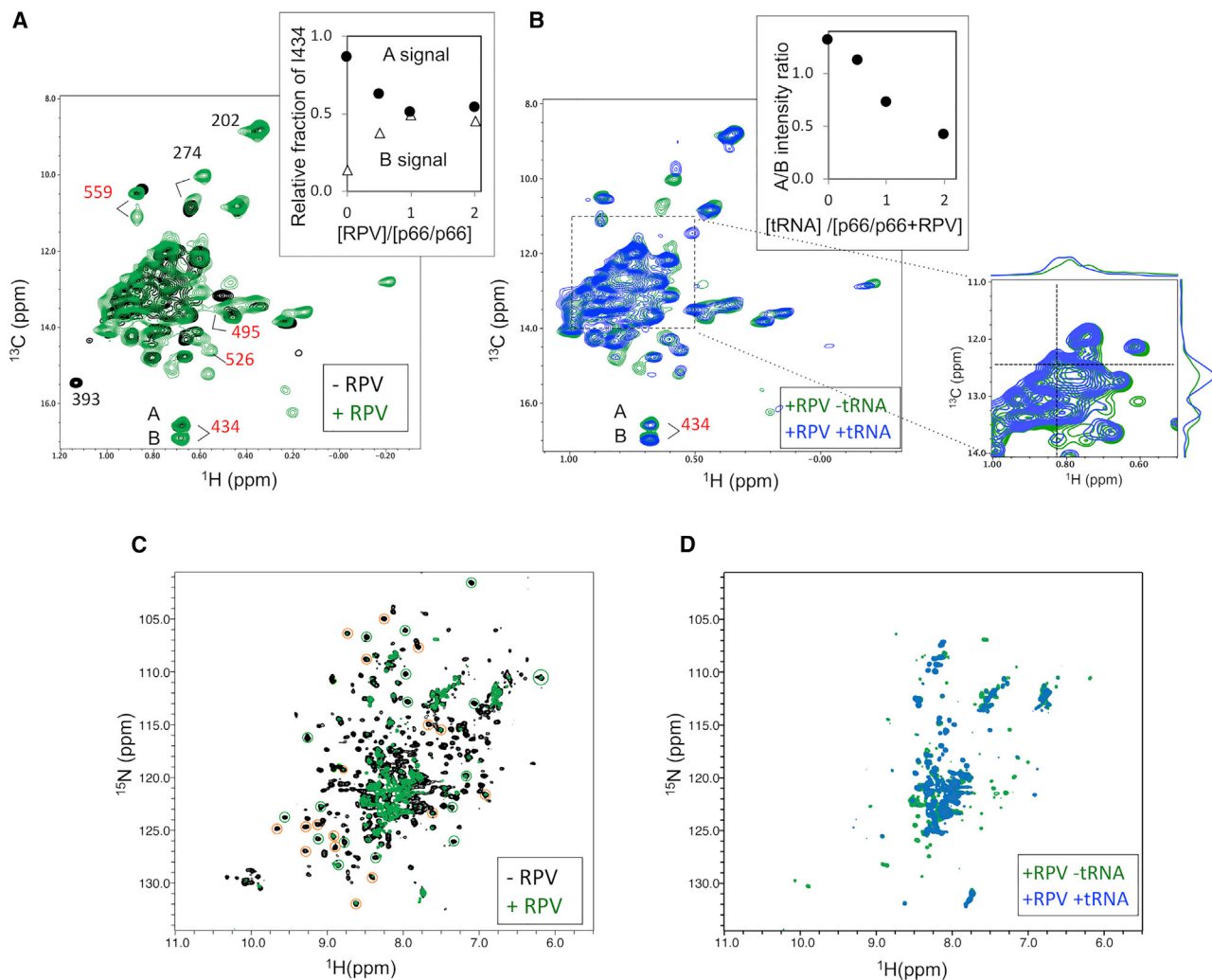


Figure 6. ^1H - ^{13}C SOFAST-HMQC NMR Spectra of $[\text{U}-^2\text{H}]$, Ile $\delta 1$ - $^{13}\text{CH}_3$ p66/p66

HMQC spectra (A) in the absence (black) or presence (green) of RPV, and (B) in the presence of RPV (green) or RPV plus tRNA^{Lys3} (blue), recorded at 35°C, and ^1H - ^{15}N TROSY-HSQC NMR spectra of $[\text{U}-^2\text{H}]$, ^{15}N p66/p66 (C) in the absence (black) or presence (green) of RPV, and (D) in the presence of RPV (green) or RPV plus tRNA^{Lys3} (blue), recorded at 20°C. In (A and B), inset graphs show relative intensity changes of residue 434 resonances (A and B) at different $[\text{RPV}]:[\text{p66}/\text{p66}]$ or $[\text{tRNA}]:[\text{p66}/\text{p66}+\text{RPV}]$ ratios. In (B), a selected region (box) is shown at high threshold level with slices taken at the dashed lines, the cross-section of which is nearly at a random coil position. In (C), resonances that overlap with previously assigned resonances of the isolated thumb and RNH domains are circled by green and orange colors, respectively (Sharaf et al., 2014).

data show that NNRTIs, which induce p66/p66 homodimer formation, have minimal impact on p66 processing, suggesting that p66/p66 homodimer formation alone is not sufficient to drive proteolytic processing of p66 to p51, and the presence of tRNA^{Lys3} introduces a change that allows efficient processing.

Probing RPV-Bound p66/p66 Conformation in the Absence and Presence of tRNA^{Lys3}

To further probe the RPV-induced conformational changes in p66/p66, we first titrated $[\text{U}-^2\text{H}]$, Ile $\delta 1$ - $^{13}\text{CH}_3$ p66/p66 with increasing concentrations of RPV and monitored chemical shifts of the protein by ^1H - ^{13}C SOFAST-HMQC experiments. We found that some signal intensities in the RNH domain decreased and new signals appeared (Figure 6A). The most salient example is residue I434. In the apo form, residue 434 appeared as a sin-

gle isolated resonance near 16 ppm ^{13}C chemical shift (bottom of the spectrum); the intensity of this resonance (labeled A) decreased while a new resonance, B, appeared with increasing RPV concentration (Figure 6A). An analysis of the intensity change indicates a binding ratio $[\text{RPV}]:[\text{p66}/\text{p66}]$ of 1:1 (Figure 6A, graph). This observation of two sets of signals in RPV-bound p66/p66 suggests introduction of conformational asymmetry in the RNH domain of p66/p66 (or rigorously speaking, chemical shift), with two folded RNH domains that have different resonance positions relative to each other. Despite this asymmetry, introduced by inhibitor binding, *in vitro* RT maturation of RPV-p66/p66 was similar to p66/p66 in the absence of RPV, with low efficiency (Figure 5). This suggests that conformational asymmetry alone is not sufficient to facilitate efficient RT maturation.

Next, we titrated p66/p66-RPV with tRNA^{Lys3}, and monitored the p66 signals by ¹H-¹³C SOFAST-HMQC experiments, to gain further insight into the conformational changes that facilitate RT maturation (Figure 6B). We found that resonance A of residue 434 decreased in signal intensity while resonance B remained stable, indicating that tRNA^{Lys3} influences the A RNH domain in p66/p66 homodimer more than the B RNH domain (Figure 6B) (described below). The observed change in the chemical shift of resonance A suggests either conformational change of a region that includes I434 or changes of the chemical environment surrounding I434, presumably by domain orientation changes or by interaction with tRNA^{Lys3}. Consistent with tRNA^{Lys3} titration into p66/p66 alone (Figure 3A), tRNA^{Lys3} titration into p66/p66-RPV produced a slight increase in the resonances located in the random coiled region (Figure 6B, side panel).

In contrast to the ¹H-¹³C SOFAST-HMQC experiments of Ile δ 1 methyl groups, ¹H-¹⁵N TROSY-HSQC did not show clear changes in signal positions for the amide backbone signals of p66/p66 upon RPV interaction; instead, only a reduction of amide backbone signal intensity was observed, including some of the thumb and RNH domain resonances (Figure 6C). This is consistent with the fact that the NNRTI-bound p66/p66 conformation is similar to that of the NNRTI-bound heterodimer (Sharaf et al., 2017), including possibly reduced RNH and thumb domain mobility, and that NNRTI rigidifies the thumb conformation (Ivetac and McCammon, 2011; Schauer et al., 2014; Termiz and Bahar, 2002). tRNA^{Lys3} interaction with p66/p66-RPV further reduced molecular tumbling (Figure 6D), presumably due to dimer-oligomer equilibrium as seen in the SEC (Figures 4F and 4G).

In Figure 7, we summarize the observed NMR spectral changes, recorded at 35°C, for three different residues in the RNH domain of RT: I434, I495, and I559. As described above, I434 exhibits a single signal in the spectrum of p66/p66 (resonance A; Figure 7A, top), under experimental conditions in which ~80% of the p66 exists as a homodimer (Sharaf et al., 2014; Sluis-Cremer et al., 2000; Venezia et al., 2006, 2009). Upon RPV binding, a second I434 signal is observed (resonance B; Figure 7B, top). Addition of tRNA^{Lys3} eliminates resonance A and slightly changes the position of resonance B (resonance B'; Figure 7C, top). This resonance B' is similar to that observed in the partially processed RT, i.e., containing both p66/p66 and p66/p51 (Figure 7D, top). Although we do not know where the A resonance moved, we note that the resonance at the random coil position was increased in the presence of tRNA^{Lys3}. Thus, it is possible that the region including I434 in subunit A (light yellow RNH domain in the cartoon of Figure 7C) is unfolded. Importantly, resonance A is absent in the p66/p51 spectrum, while resonance B' is clearly present (Figure 7E, top). Similar spectral changes were also observed at RNH domain residues I495 and I559 (Figure 7, the second and third rows). However, the chemical resonance at I495 in the p66/p51 heterodimer does not line up with the same chemical shift as the partially digested p66 (Figures 7D and 7E, the second row), suggesting that this residue may undergo internal dynamics. Data recorded at 20°C indicate similar tendencies but exhibit more conformers, presumably due to slower rates of exchange (Figure S5).

Based on these spectral changes and previous ¹⁹F NMR that monitored residue 181 located at the NNRTI binding pocket of

p66/p51 and p66/p66 (Sharaf et al., 2016, 2017), the following scenario for p66/p66 conformational changes is derived (cartoons at the bottom of Figures 7A–7E). (1) p66/p66 is in equilibrium with p66 monomer and exhibits one set of stable signals, with the two RNH domains in the p66/p66 homodimer folded and symmetrical. (2) RPV binding induces some asymmetry, or conformational change, in one RNH domain to create an environment similar to that of the RNH domain in p66/p51, such that the p51-RNH site is protected (orange in the cartoon of Figure 7C). However, this conformational change is not sufficient to drive proteolytic processing. (3) tRNA interaction affects the A peak within the RNH domain (yellow in the cartoon of Figure 7C), which is the subunit that is cleaved by PR (note the reduced intensity of peak A in Figures 7D compared with 7A). Overall, tRNA^{Lys3} generates partial unfolding of the protein, presumably of the RNH domain region, in the presence and absence of RPV (Figure 3).

Knockdown of KARS in 293T Cells Affects Intracellular RT Processing and Reduces Virus Particle Production

Collectively, our data underscore that tRNA^{Lys3} binding to the p66/p66 RT homodimer triggers the necessary conformational changes that facilitate PR access to the cleavage site. During the HIV-1 life cycle, tRNA^{Lys3} is essential as a primer for reverse transcription reaction and is recruited into the budding virus through its interaction with KARS and Gag-Pol (Cen et al., 2001, 2002; Khorchid et al., 2000; Kleiman and Cen, 2004; Kleiman et al., 2010; Mak et al., 1994, 1997). However, it is unknown whether tRNA^{Lys3} affects RT maturation during viral replication. Thus, to investigate the role of tRNA^{Lys3} in RT maturation, we knocked down KARS expression in 293T cells by small interfering RNA (siRNA), and then transfected these cells with a full-length replication competent molecular clone of HIV-1 (HIV-1_{LAI}). We anticipated that this knockdown would impact virus replication, Gag-Pol polyprotein processing in the host cell and/or virus, and possibly the formation of the reverse transcription initiation complex. It has been previously shown that KARS knockdown does not alter general protein translation (Nam et al., 2015). Forty-eight hours after HIV-1_{LAI} transfection, we evaluated RT expression in both the 293T cells and in purified viral particles.

The siRNA knockdown of KARS expression in the 293T cells was stable for the duration of the experiment (Figure 8A). We found intracellular accumulation of RT that was not observed in the control cells (Figures 8B and 8C). Interestingly, the KARS knockdown cells accumulated p66, which did not appear to be efficiently processed to p51 by HIV-1 PR (Figures 8B and 8C), indicating a possible effect of tRNA^{Lys3} on RT maturation within the cellular environment. Compared with control cells, KARS knockdown resulted in a significant reduction in viral particle production, as assessed by quantification of p24 (Figure 8D). However, in the viral particles that were produced from KARS knockdown cells, the p66:p51 ratio was 1:1 (Figures 8E and 8F), with no difference in relative infectivity (as measured in TZM-bl cells) between the viruses generated from the control and KARS knockdown cell lines (Figure 8G). These observations may suggest a role for tRNA^{Lys3} in viral assembly, which is beyond the scope of the current study. We could not measure tRNA^{Lys3} levels in the

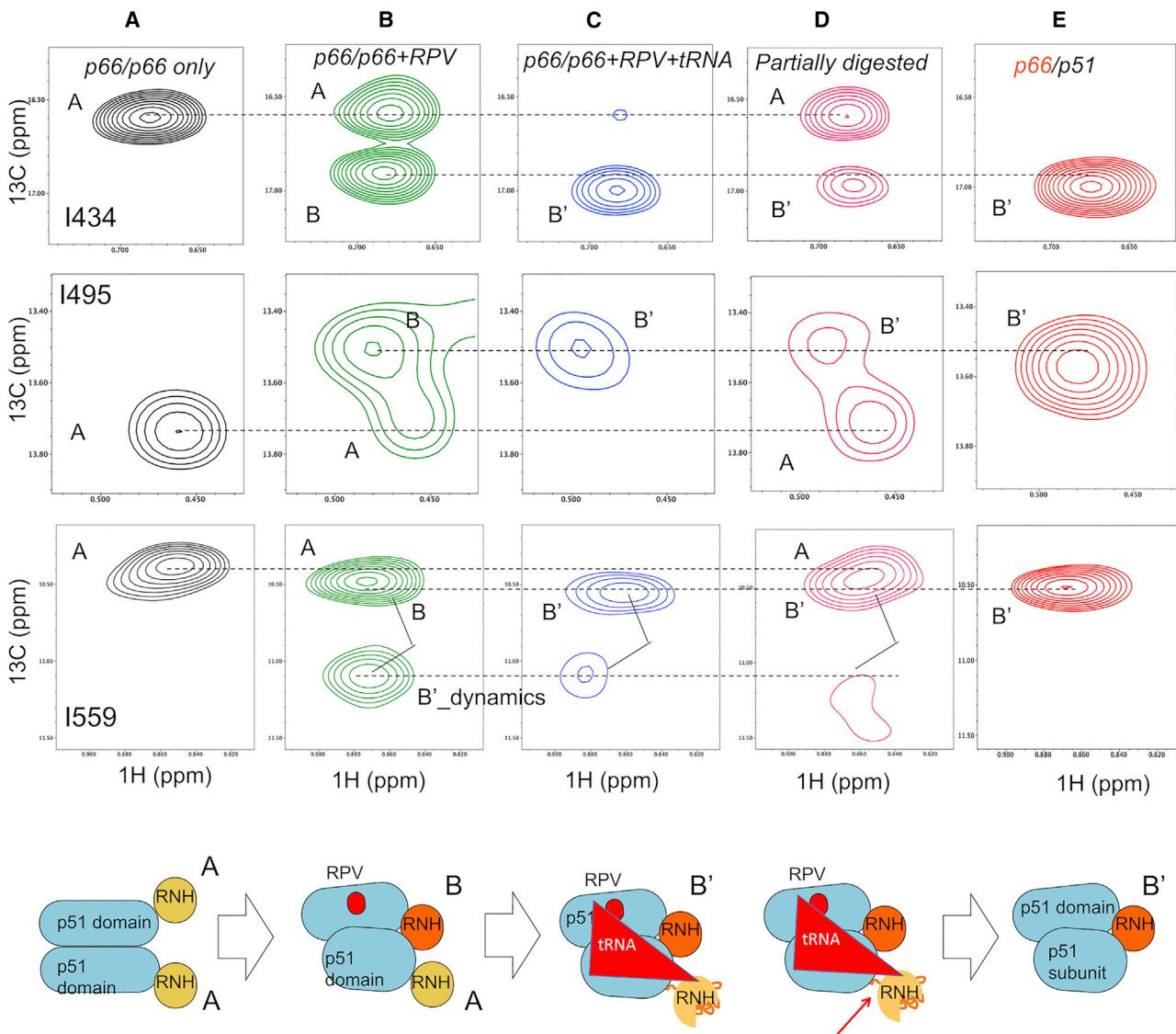


Figure 7. Overview of the Observed Signal Patterns of p66/p66 RNH Domain Residues I434, I495, and I559

(A) p66/p66 only, (B) p66/p66 + RPV, (C) p66/p66 + RPV + tRNA, (D) partially digested p66/p66 sample, and (E) p66/p51 in which only the p66 subunit is [U-²H] and Ile δ1-[¹³CH₃] labeled. All the spectra were recorded at 35°C. Cartoon at the bottom indicates conformational changes deduced from the observed spectra in each condition. The designation A in the spectra indicates resonance positions stemming from the p66/p66 homodimer, while B and B' indicate newly generated resonance upon RPV interaction and partial digestion of p66/p66, respectively. See also Figure S5.

viral particles produced by KARS knockdown cell lines due to low virus production of these cells.

DISCUSSION

In all structures of the mature p66/p51 heterodimer, the p51-RNH cleavage site is sequestered in a β sheet within the RNH domain and is inaccessible to PR (Figure 1B). Thus, the pathways involved in maturation of the asymmetric p66/p51 heterodimer are unknown. Using an *in vitro* RT maturation assay, we previously demonstrated that interaction of tRNA^{Lys3} with the p66/p66 homodimer enhances specific cleavage by PR at the

p51-RNH cleavage site, resulting in p66/p51 formation (Ilin et al., 2018). The mechanisms by which tRNA^{Lys3} enhances p66/p51 heterodimer production, however, are unclear and could involve its ability to increase p66/p66 homodimer formation and/or introduce conformational changes, particularly in the RNH domain of RT, which facilitate PR-mediated processing of p66 to p51. Thus, we assessed the impact of tRNA^{Lys3} interaction on p66/p66 conformation in solution using ¹H-¹³C HMQC NMR of ³C δ1-Ile signals of p66, to assess specific signals with high sensitivity, and using ¹H-¹⁵N TROSY-HSQC NMR of [U-²H,¹⁵N]p66, to gain insight into overall conformational changes in the protein.

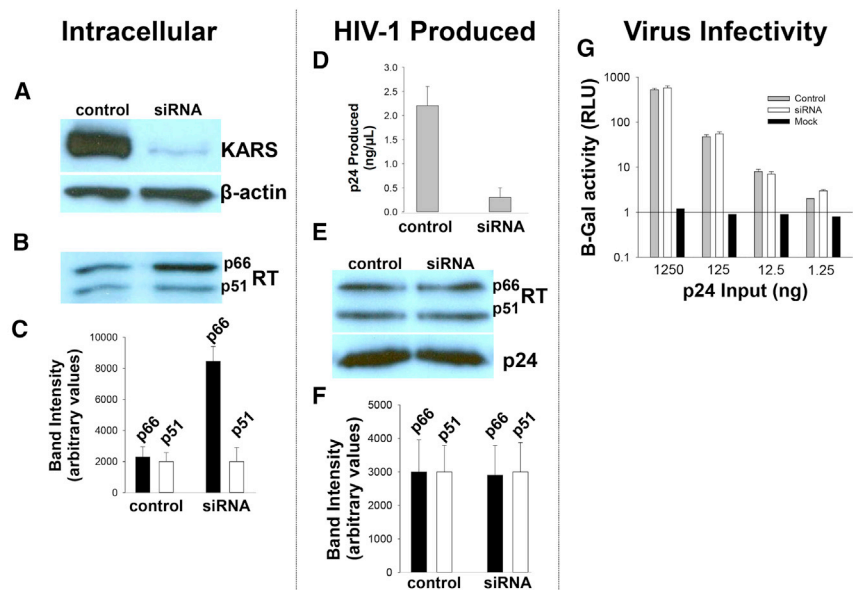


Figure 8. siRNA-Mediated Knockdown of KARS in 293T Cells

(A) Western blot analysis of KARS and B-actin expression in 293T cells 48 h after HIV-1 transfection; (B) western blot of intracellular RT expression; (C) densitometric analysis of (B); amount of HIV-1 produced, as assessed by p24, from the KARS knockdown and control 293T cells; (E) virion-associated RT and p24; (F) densitometric analysis of (E); single-cycle infectivity of HIV-1 generated from KARS knockdown and control 293T cells as assessed in TZM-bL cells. The data in (C, D, F, and G) are reported as the mean \pm SE from three independent experiments.

The results indicate a partial unfolding of p66/p66, reduction of thumb domain motion, and reduction in the mobility of at least one RNH domain upon tRNA^{Lys3} interaction (Figure 3). In addition, a slight increase in the signal intensity proximal to the random coil position of the Ile- δ 1 methyl group was observed (Figure 3). In large protein NMR, even a small number of fragments can give significant signals, because of the small rotational correlation time of fragments compared with that of the large protein. Such fragments could be introduced to a sample upon cleavage by contaminated *E. coli* enzyme; however, in this study, the increases in the unfolded signals detected in the ¹H-¹³C and ¹H-¹⁵N data are not due to generation of fragmented protein products, as shown in the SDS gels (Figures S6 and S7).

To reduce the p66 monomer fraction in our samples, we utilized NNRTIs that are potent chemical enhancers of p66/p66 homodimer formation (Hughes, 2001; Tachedjian et al., 2001). Using an *in vitro* maturation assay (Figure 5), we unequivocally show that NNRTIs do not facilitate proteolytic processing of p66 to p51, whereas addition of tRNA^{Lys3} to the NNRTI-bound p66/p66 resulted in efficient cleavage. Our NMR experiments show that NNRTI binding induced conformational changes in p66/p66 homodimer that extended to the RNH domains (Figure 6A). However, these conformational changes were not sufficient to induce efficient PR processing at the p51-RNH site (Figure 5C). Indeed, the addition of tRNA^{Lys3} induced additional changes particularly in the RNH domain (Figure 6B), with an increase in the unfolded resonance similar to that observed in the experiments without RPV. Collectively, these data show that specific conformational changes in the p66/p66 homodimer, enhanced by nucleic acid, are needed for efficient RT maturation.

In the Ile- δ 1 methyl ¹H-¹³C HMQC spectrum of p66/p66-RPV in the presence of tRNA^{Lys3}, we observed resonance changes for residues in the finger-palm and thumb domains, 202 and 274, as well as those in the RNH domain. Thus, tRNA^{Lys3} is expected to bind at the canonical nucleic acid binding site that spans the entire p51 domain in p66 (Sarafianos et al., 2001). This notion is consistent with the observed reduction in thumb

domain signals upon tRNA^{Lys3} binding to p66, monitored by ¹H-¹⁵N TROSY-HSQC NMR (Figure 3B). Previous ¹⁹F NMR studies have suggested that the NNRTI binding pocket of p66/p66 is similar to that of p66/p51 (Sharaf et al., 2016, 2017). If a p66/p51-like structure is present in the p66/p66-RPV form, our observation that the p66/p66-RPV-bound conformation is asymmetric but not ideal for p66/p51 production in the absence of tRNA^{Lys3} suggests a steric effect of tRNA^{Lys3} on one of the RNH domains. Since we were unable to identify the specific region that undergoes partial unfolding, the RNH domain signal observed in the tRNA^{Lys3}-bound p66/p66 in the ¹H-¹⁵N TROSY-HSQC NMR spectrum (Figure 3B) could correspond to domains A or B in the Ile- δ 1 methyl ¹H-¹³C HMQC of Figure 6B or to the tRNA^{Lys3}-p66 monomer form. In either case, our data do not support the model that p66/p66 alone, in the absence of nucleic acid or PR, slowly changes conformation in solution (Zheng et al., 2014, 2015, 2016), as we did not observe such a conformational change. Even if there is a minor conformer, it may be separated by a high energy barrier from the major population in p66/p66 alone.

During the HIV-1 life cycle, tRNA^{Lys3} is recruited into the budding virus through its interaction with KARS and Gag-Pol (Cen et al., 2001, 2002; Khorchid et al., 2000; Kleiman and Cen, 2004; Kleiman et al., 2010; Mak et al., 1994, 1997). To investigate the role of tRNA^{Lys3} in RT maturation, we knocked down KARS expression in 293T cells by siRNA, and then transfected these cells with a full-length replication competent molecular clone of HIV-1 (HIV-1_{LA1}). Interestingly, we found intracellular accumulation of inefficiently processed RT in cells with reduced KARS. Since KARS knockdown significantly reduced the amount of virus production, we think that the accumulated Gag-Pol and the products in the cell showed such difference in RT maturation in the intracellular environment. Thus, the result is not a direct evidence of the RT maturation in virus, but suggests a possible role of KARS in the intracellular maturation of RT and supports application of tRNA^{Lys3} in our *in vitro* data.

The reduction of the amount of virus production is consistent with the notion that KARS is important for viral packaging of tRNA^{Lys3} and Gag-Pol (Cen et al., 2004; Guo et al., 2003). The virus that was produced from the KARS knockdown cells, however, contained p66/p51 RT and exhibited similar infectivity to the control virus. While we observed robust knockdown of

KARS in the 293T cells, there was residual protein expression, which may have been sufficient to facilitate some virus production. However, how tRNA^{Lys3} affects viral packaging is beyond the scope of the current study. Similarly, there are studies that have investigated the order of PR cleavage sites in Gag-Pol using different systems (Abram et al., 2010; Pettit et al., 2004, 2005a, 2005b). In this regard, our study does not address the entire RT maturation pathway from Gag-Pol processing to p66/p51 production, but illuminates the RT conformational characteristics in relation to functional heterodimer maturation.

STAR★METHODS

Detailed methods are provided in the online version of this paper and include the following:

- **KEY RESOURCES TABLE**
- **LEAD CONTACT AND MATERIALS AVAILABILITY**
- **EXPERIMENTAL MODEL AND SUBJECT DETAILS**
 - Bacterial Strains
 - Cells
 - Viruses
- **METHOD DETAILS**
 - In Vitro RT Maturation Experiments
 - In Vitro tRNA Transcription
 - Analytical Size Exclusion Chromatography to Monitor p66/p66-tRNA Interaction
 - Sample Preparation for NMR Experiments
 - NMR Experiments
 - KARS Knockdown Experiments
- **QUANTIFICATION AND STATISTICAL ANALYSIS**
- **DATA AND CODE AVAILABILITY**

SUPPLEMENTAL INFORMATION

Supplemental Information can be found online at <https://doi.org/10.1016/j.str.2019.08.004>.

ACKNOWLEDGMENTS

We thank Michel Guerrero for technical support and Teresa Brosenitsch for reading the manuscript. This study was supported by grants from the NIH (R01GM105401 to R.I., U54AI150472 and R01GM118012 to S.G.S., R01GM068406 to N.S.C., and P50AI150481 to R.I. and N.S.C.), and the MEXT-Supported Program for the Strategic Research Foundation at Private Universities in Japan (the term, 2011–2015, to G.K.).

AUTHOR CONTRIBUTIONS

Conceptualization, R.L.S., S.G.S., N.S.C., and R.I.; Investigation, R.L.S., T.V.I., Z.X., N.S.G., G.K., and M.A.P.; Formal Analysis, R.L.S., T.V.I., Z.X., N.S.G., and G.K.; Writing – Original Draft, R.L.S. and R.I.; Writing – Review & Editing, S.G.S., N.S.C., and R.I.; Supervision, S.G.S., N.S.C., and R.I.; Funding Acquisition, G.K., S.G.S., N.S.C., and R.I.

DECLARATION OF INTERESTS

The authors declare no competing interests.

Received: February 13, 2019

Revised: July 10, 2019

Accepted: August 9, 2019

Published: August 27, 2019

REFERENCES

- Abram, M.E., and Parniak, M.A. (2005). Virion instability of human immunodeficiency virus type 1 reverse transcriptase (RT) mutated in the protease cleavage site between RT p51 and the RT RNase H domain. *J. Virol.* 79, 11952–11961.
- Abram, M.E., Sarafianos, S.G., and Parniak, M.A. (2010). The mutation T477A in HIV-1 reverse transcriptase (RT) restores normal proteolytic processing of RT in virus with Gag-Pol mutated in the p51-RNH cleavage site. *Retrovirology* 7, 6.
- Bakhanashvili, M., and Hizi, A. (1994). Interaction of the reverse transcriptase of human immunodeficiency virus type 1 with DNA. *Biochemistry* 33, 12222–12228.
- Bavand, M.R., Wagner, R., and Richmond, T.J. (1993). HIV-1 reverse transcriptase: polymerization properties of the p51 homodimer compared to the p66/p51 heterodimer. *Biochemistry* 32, 10543–10552.
- Braz, V.A., Holladay, L.A., and Barkley, M.D. (2010). Efavirenz binding to HIV-1 reverse transcriptase monomers and dimers. *Biochemistry* 49, 601–610.
- Cen, S., Javanbakht, H., Kim, S., Shiba, K., Craven, R., Rein, A., Ewalt, K., Schimmel, P., Musier-Forsyth, K., and Kleiman, L. (2002). Retrovirus-specific packaging of aminoacyl-tRNA synthetases with cognate primer tRNAs. *J. Virol.* 76, 13111–13115.
- Cen, S., Javanbakht, H., Niu, M., and Kleiman, L. (2004). Ability of wild-type and mutant lysyl-tRNA synthetase to facilitate tRNA(Lys) incorporation into human immunodeficiency virus type 1. *J. Virol.* 78, 1595–1601.
- Cen, S., Khorchid, A., Javanbakht, H., Gabor, J., Stello, T., Shiba, K., Musier-Forsyth, K., and Kleiman, L. (2001). Incorporation of lysyl-tRNA synthetase into human immunodeficiency virus type 1. *J. Virol.* 75, 5043–5048.
- Chattopadhyay, D., Evans, D.B., Deibel, M.R., Jr., Vosters, A.F., Eckenrode, F.M., Einspahr, H.M., Hui, J.O., Tomasselli, A.G., Zurcher-Neely, H.A., Heinrikson, R.L., et al. (1992). Purification and characterization of heterodimeric human immunodeficiency virus type 1 (HIV-1) reverse transcriptase produced by in vitro processing of p66 with recombinant HIV-1 protease. *J. Biol. Chem.* 267, 14227–14232.
- Clark, A.D., JacoboMolina, A., Clark, P., Hughes, S.H., and Arnold, E. (1995). Crystallization of human immunodeficiency virus type 1 reverse transcriptase with and without nucleic acid substrates, inhibitors, and an antibody fab fragment. *Method Enzymol.* 262, 171–185.
- Coffin, J.M., Hughes, S.H., and Varmus, H.E. (1997). *Retroviruses* (old Spring Harbor Laboratory Press).
- Davies, J.F., 2nd, Hostomska, Z., Jordan, S.R., and Matthews, D.A. (1991). Crystal structure of the ribonuclease H domain of HIV-1 reverse transcriptase. *Science* 252, 88–95.
- Delaglio, F., Grzesiek, S., Vuister, G.W., Zhu, G., Pfeifer, J., and Bax, A. (1995). NMRPipe: a multidimensional spectral processing system based on UNIX pipes. *J. Biomol. NMR* 6, 277–293.
- Divita, G., Rittinger, K., Geourjon, C., Deleage, G., and Goody, R.S. (1995). Dimerization kinetics of HIV-1 and HIV-2 reverse transcriptase: a two step process. *J. Mol. Biol.* 245, 508–521.
- Figueiredo, A., Moore, K.L., Mak, J., Sluis-Cremer, N., de Bethune, M.P., and Tachedjian, G. (2006). Potent nonnucleoside reverse transcriptase inhibitors target HIV-1 Gag-Pol. *PLoS Pathog.* 2, e119.
- Giacobbi, N.S., and Sluis-Cremer, N. (2017). In vitro cross-resistance profiles of Rilpivirine, Dapivirine, and MIV-150, nonnucleoside reverse transcriptase inhibitor microbicides in clinical development for the prevention of HIV-1 infection. *Antimicrob. Agents Chemother.* 61, <https://doi.org/10.1128/AAC.00277-17>.
- Guo, F., Cen, S., Niu, M., Javanbakht, H., and Kleiman, L. (2003). Specific inhibition of the synthesis of human Lysyl-tRNA synthetase results in decreases in tRNA^{Lys} incorporation, Trna3^{Lys} annealing to viral RNA, and viral infectivity in human immunodeficiency virus type 1. *J. Virol.* 77, 9817–9822.
- Hughes, S.H. (2001). Molecular matchmaking: NNRTIs can enhance the dimerization of HIV type 1 reverse transcriptase. *Proc. Natl. Acad. Sci. U S A* 98, 6991–6992.

- Ilna, T.V., Slack, R.L., Elder, J.H., Sarafianos, S.G., Parniak, M.A., and Ishima, R. (2018). Effect of tRNA on the maturation of HIV-1 reverse transcriptase. *J. Mol. Biol.* **430**, 1891–1900.
- Ivetac, A., and McCammon, J.A. (2011). Molecular recognition in the case of flexible targets. *Curr. Pharm. Des.* **17**, 1663–1671.
- Jacobo-Molina, A., and Arnold, E. (1991). HIV reverse transcriptase structure-function relationships. *Biochemistry* **30**, 6351–6356.
- Jacobo-Molina, A., Ding, J., Nanni, R.G., Clark, A.D.J., Lu, X., Tantillo, C., Williams, R.L., Kamer, G., Ferris, A.L., Clark, P., et al. (1993). Crystal structure of human immunodeficiency virus type 1 reverse transcriptase complexed with double-stranded DNA at 3.0 Å resolution shows bent DNA. *Proc. Natl. Acad. Sci. U S A* **90**, 6320–6324.
- Jiang, M., Mak, J., Ladha, A., Cohen, E., Klein, M., Rovinski, B., and Kleiman, L. (1993). Identification of tRNAs incorporated into wild-type and mutant human immunodeficiency virus type 1. *J. Virol.* **67**, 3246–3253.
- Jiang, M., Mak, J., Wainberg, M.A., Parniak, M.A., Cohen, E., and Kleiman, L. (1992). Variable tRNA content in HIV-1III_B. *Biochem. Biophys. Res. Commun.* **185**, 1005–1015.
- Johnson, B.A. (2004). Using NMRView to visualize and analyze the NMR spectra of macromolecules. *Methods Mol. Biol.* **278**, 313–352.
- Katz, R.A., and Skalka, A.M. (1994). The retroviral enzymes. *Annu. Rev. Biochem.* **63**, 133–173.
- Khan, S.N., Persons, J.D., Paulsen, J.L., Guerrero, M., Schiffer, C.A., Kurt-Yilmaz, N., and Ishima, R. (2018). Probing structural changes among analogous inhibitor-bound forms of HIV-1 protease and a drug-resistant mutant in solution by nuclear magnetic resonance. *Biochemistry* **57**, 1652–1662.
- Khorchid, A., Javanbakht, H., Wise, S., Halwani, R., Parniak, M.A., Wainberg, M.A., and Kleiman, L. (2000). Sequences within Pr160gag-pol affecting the selective packaging of primer tRNA(Lys3) into HIV-1. *J. Mol. Biol.* **299**, 17–26.
- Kleiman, L., Caudry, S., Boulerice, F., Wainberg, M.A., and Parniak, M.A. (1991). Incorporation of tRNA into normal and mutant HIV-1. *Biochem. Biophys. Res. Commun.* **174**, 1272–1280.
- Kleiman, L., and Cen, S. (2004). The tRNALys packaging complex in HIV-1. *Int. J. Biochem. Cell Biol.* **36**, 1776–1786.
- Kleiman, L., Jones, C.P., and Musier-Forsyth, K. (2010). Formation of the tRNALys packaging complex in HIV-1. *FEBS Lett.* **584**, 359–365.
- Kohlstaedt, L.A., Wang, J., Friedman, J.M., Rice, P.A., and Steitz, T.A. (1992). Crystal structure at 3.5 Å resolution of HIV-1 reverse transcriptase complexed with an inhibitor. *Science* **256**, 1783–1790.
- Lansdon, E.B., Brendza, K.M., Hung, M., Wang, R., Mukund, S., Jin, D., Birkus, G., Kutty, N., and Liu, X. (2010). Crystal structures of HIV-1 reverse transcriptase with etravirine (TMC125) and rilpivirine (TMC278): implications for drug design. *J. Med. Chem.* **53**, 4295–4299.
- Le Grice, S.F., and Gruninger-Leitch, F. (1990). Rapid purification of homodimer and heterodimer HIV-1 reverse transcriptase by metal chelate affinity chromatography. *Eur. J. Biochem.* **187**, 307–314.
- Lindhofer, H., von der Helm, K., and Nitschko, H. (1995). In vivo processing of Pr160gag-pol from human immunodeficiency virus type 1 (HIV) in acutely infected, cultured human T-lymphocytes. *Virology* **214**, 624–627.
- Lowe, D.M., Aitken, A., Bradley, C., Darby, G.K., Larder, B.A., Powell, K.L., Purifoy, D.J., Tisdale, M., and Stammers, D.K. (1988). HIV-1 reverse transcriptase: crystallization and analysis of domain structure by limited proteolysis. *Biochemistry* **27**, 8884–8889.
- Mak, J., Jiang, M., Wainberg, M.A., Hammarskjold, M.-L., Rekosh, D., and Kleiman, L. (1994). Role of Pr160gag-pol in mediating the selective incorporation of tRNALys into human immunodeficiency virus type 1 particles. *J. Virol.* **68**, 2065–2072.
- Mak, J., Khorchid, A., Cao, Q., Huang, Y., Lowy, I., Parniak, M.A., Prasad, V.R., Wainberg, M.A., and Kleiman, L. (1997). Effects of mutations in Pr160gag-pol upon tRNA(Lys3) and Pr160gag-pol incorporation into HIV-1. *J. Mol. Biol.* **265**, 419–431.
- Mattei, S., Anders, M., Konvalinka, J., Krausslich, H.G., Briggs, J.A., and Muller, B. (2014). Induced maturation of human immunodeficiency virus. *J. Virol.* **88**, 13722–13731.
- Miller, J.T., Khvorova, A., Scaringe, S.A., and Le Grice, S.F. (2004). Synthetic tRNALys,3 as the replication primer for the HIV-1HXB2 and HIV-1Mal genomes. *Nucleic Acids Res.* **32**, 4687–4695.
- Nam, S.H., Kim, D., Lee, M.S., Lee, D., Kwak, T.K., Kang, M., Ryu, J., Kim, H.J., Song, H.E., Choi, J., et al. (2015). Noncanonical roles of membranous lysyl-tRNA synthetase in transducing cell-substrate signaling for invasive dissemination of colon cancer spheroids in 3D collagen I gels. *Oncotarget* **6**, 21655–21674.
- Nicholson, L.K., Kay, L.E., Baldissari, D.M., Arango, J., Young, P.E., Bax, A., and Torchia, D.A. (2002). Dynamics of methyl groups in proteins as studied by proton-detected carbon-13 NMR spectroscopy. Application to the leucine residues of staphylococcal nuclease. *Biochemistry* **31**, 5253–5263.
- Pavon-Eternod, M., Wei, M., Pan, T., and Kleiman, L. (2010). Profiling non-lysyl tRNAs in HIV-1. *RNA* **16**, 267–273.
- Pettit, S.C., Clemente, J.C., Jeung, J.A., Dunn, B.M., and Kaplan, A.H. (2005a). Ordered processing of the human immunodeficiency virus type 1 GagPol precursor is influenced by the context of the embedded viral protease. *J. Virol.* **79**, 10601–10607.
- Pettit, S.C., Everitt, L.E., Choudhury, S., Dunn, B.M., and Kaplan, A.H. (2004). Initial cleavage of the human immunodeficiency virus type 1 GagPol precursor by its activated protease occurs by an intramolecular mechanism. *J. Virol.* **78**, 8477–8485.
- Pettit, S.C., Lindquist, J.N., Kaplan, A.H., and Swanstrom, R. (2005b). Processing sites in the human immunodeficiency virus type 1 (HIV-1) Gag-Pro-Pol precursor are cleaved by the viral protease at different rates. *Retrovirology* **2**, 66.
- Sarafianos, S.G., Das, K., Tantillo, C., Clark, A.D., Jr., Ding, J., Whitcomb, J.M., Boyer, P.L., Hughes, S.H., and Arnold, E. (2001). Crystal structure of HIV-1 reverse transcriptase in complex with a polypurine tract RNA:DNA. *EMBO J.* **20**, 1449–1461.
- Schauer, G.D., Huber, K.D., Leuba, S.H., and Sluis-Cremer, N. (2014). Mechanism of allosteric inhibition of HIV-1 reverse transcriptase revealed by single-molecule and ensemble fluorescence. *Nucleic Acids Res.* **42**, 11687–11696.
- Sharaf, N.G., Ishima, R., and Gronenborn, A.M. (2016). Conformational plasticity of the NNRTI-binding pocket in HIV-1 reverse transcriptase—a fluorine NMR study. *Biochemistry* **55**, 3864–3873.
- Sharaf, N.G., Poliner, E., Slack, R.L., Christen, M.T., Byeon, I.J., Parniak, M.A., Gronenborn, A.M., and Ishima, R. (2014). The p66 immature precursor of HIV-1 reverse transcriptase. *Proteins* **82**, 2343–2352.
- Sharaf, N.G., Xi, Z., Ishima, R., and Gronenborn, A.M. (2017). The HIV-1 p66 homodimeric RT exhibits different conformations in the binding-competent and -incompetent NNRTI site. *Proteins* **85**, 2191–2197.
- Sharma, S.K., Fan, N., and Evans, D.B. (1994). Human immunodeficiency virus type 1 (HIV-1) recombinant reverse transcriptase. Asymmetry in p66 subunits of the p66/p66 homodimer. *FEBS Lett.* **343**, 125–130.
- Sherlin, L.D., Bullock, T.L., Nissan, T.A., Perona, J.J., Lariviere, F.J., Uhlenbeck, O.C., and Scaringe, S.A. (2001). Chemical and enzymatic synthesis of tRNAs for high-throughput crystallization. *RNA* **7**, 1671–1678.
- Shi, C., and Mellors, J.W. (1997). A recombinant retroviral system for rapid in vivo analysis of human immunodeficiency virus type 1 susceptibility to reverse transcriptase inhibitors. *Antimicrob. Agents Chemother.* **41**, 2781–2785.
- Sluis-Cremer, N., Arion, D., Abram, M.E., and Parniak, M.A. (2004). Proteolytic processing of an HIV-1 pol polyprotein precursor: insights into the mechanism of reverse transcriptase p66/p51 heterodimer formation. *Int. J. Biochem. Cell Biol.* **36**, 1836–1847.
- Sluis-Cremer, N., Dmitrienko, G.I., Balzarini, J., Camarasa, M.J., and Parniak, M.A. (2000). Human immunodeficiency virus type 1 reverse transcriptase dimer destabilization by 1-[spiro[4'-amino-2',2'-dioxo-1',2'-oxathiole-5',3'-[2',5'-bis-O-(tert-butylidimethylsilyl)-beta-D-ribofuranosyl]]]-3-ethylthymine. *Biochemistry* **39**, 1427–1433.
- Speck, R.R., Flexner, C., Tian, C.J., and Fu, X.F. (2000). Comparison of human immunodeficiency virus type 1 Pr55(Gag) and Pr160(Gag-Pol) processing

intermediates that accumulate in primary and transformed cells treated with peptidic and nonpeptidic protease inhibitors. *Antimicrob. Agents Chemother.* **44**, 1397–1403.

Tachedjian, G., Moore, K.L., Goff, S.P., and Sluis-Cremer, N. (2005). Efavirenz enhances the proteolytic processing of an HIV-1 pol polyprotein precursor and reverse transcriptase homodimer formation. *FEBS Lett.* **579**, 379–384.

Tachedjian, G., Orlova, M., Sarafianos, S.G., Arnold, E., and Goff, S.P. (2001). Nucleoside reverse transcriptase inhibitors are chemical enhancers of dimerization of the HIV type 1 reverse transcriptase. *Proc. Natl. Acad. Sci. U S A* **98**, 7188–7193.

Termiz, N.A., and Bahar, I. (2002). Inhibitor binding alters the directions of domain motions in HIV-1 reverse transcriptase. *Proteins* **49**, 61–70.

Tugarinov, V., Kanelis, V., and Kay, L.E. (2006). Isotope labeling strategies for the study of high-molecular-weight proteins by solution NMR spectroscopy. *Nat. Protoc.* **1**, 749–754.

Venezia, C.F., Howard, K.J., Ignatov, M.E., Holladay, L.A., and Barkley, M.D. (2006). Effects of efavirenz binding on the subunit equilibria of HIV-1 reverse transcriptase. *Biochemistry* **45**, 2779–2789.

Venezia, C.F., Meany, B.J., Braz, V.A., and Barkley, M.D. (2009). Kinetics of association and dissociation of HIV-1 reverse transcriptase subunits. *Biochemistry* **48**, 9084–9093.

Vranken, W.F., Boucher, W., Stevens, T.J., Fogh, R.H., Pajon, A., Llinas, M., Ulrich, E.L., Markley, J.L., Ionides, J., and Laue, E.D. (2005). The CCPN data

model for NMR spectroscopy: development of a software pipeline. *Proteins* **59**, 687–696.

Wapling, J., Moore, K.L., Sonza, S., Mak, J., and Tachedjian, G. (2005). Mutations that abrogate human immunodeficiency virus type 1 reverse transcriptase dimerization affect maturation of the reverse transcriptase heterodimer. *J. Virol.* **79**, 10247–10257.

Wishart, D.S., Bigam, C.G., Holm, A., Hodges, R.S., and Sykes, B.D. (1995). (1)H, (13)C and (15)N random coil NMR chemical shifts of the common amino acids. I. Investigations of nearest-neighbor effects. *J. Biomol. NMR* **5**, 332.

Zheng, X., Mueller, G.A., Kim, K., Perera, L., DeRose, E.F., and London, R.E. (2017). Identification of drivers for the metamorphic transition of HIV-1 reverse transcriptase. *Biochem. J.* **474**, 3321–3338.

Zheng, X., Perera, L., Mueller, G.A., DeRose, E.F., and London, R.E. (2015). Asymmetric conformational maturation of HIV-1 reverse transcriptase. *Elife* **4**, e06359.

Zheng, X.H., Pedersen, L.C., Gabel, S.A., Mueller, G.A., Cuneo, M.J., DeRose, E.F., Krahn, J.M., and London, R.E. (2014). Selective unfolding of one ribonuclease H domain of HIV reverse transcriptase is linked to homodimer formation. *Nucleic Acids Res.* **42**, 5361–5377.

Zheng, X.H., Pedersen, L.C., Gabel, S.A., Mueller, G.A., DeRose, E.F., and London, R.E. (2016). Unfolding the HIV-1 reverse transcriptase RNase H domain—how to lose a molecular tug-of-war. *Nucleic Acids Res.* **44**, 1776–1788.

STAR★METHODS

KEY RESOURCES TABLE

REAGENT or RESOURCE	SOURCE	IDENTIFIER
Antibodies		
Anti-KARS antibodies	Sigma Aldrich	SAB5300071
RT antigen	Abcam	RRID: AB_1139531
p24 antigen	Abcam	RRID: AB_1139527
Bacterial and Virus Strains		
Escherichia coli Rosetta 2(DE3) - Novagen	Millipore Sigma	71400
Escherichia coli BL21(DE3) - Novagen	Millipore Sigma	70235
HEK 293T cells	ATCC	CRL-3216
TZM-bl cells	NIH AIDS Reagent Program	8129
HIV-1LAI virus strain	NIH AIDS Reagent Program	2522
		N/A
Chemicals, Peptides, and Recombinant Proteins		
Rilpivirine	selleckchem	S7303
Additional Rilpivirine	NIH AIDS Reagent Program	12147
Efavirenz	NIH AIDS Reagent Program	4624
Darunavir	NIH AIDS Reagent Program	11447
Glycerol-d8	Millipore Sigma	447498-1G
² H ₂ O	Millipore Sigma	151882
dimethyl sulfoxide	Millipore Sigma	D4540-500ML
D-glucose (1,2,3,4,5,6,6-D7, 97-98%)	Cambridge Isotope Lab	DLM-2062-1
α-ketobutyric acid, sodium salt (methyl 13C; 3,3-D2)	Cambridge Isotope Lab	CDLM-7318
¹⁵ NH ₄ Cl	Cambridge Isotope Lab	NLM-467-5
dimethyl sulfoxide-d6	Cambridge Isotope Lab	DLM-10-5X1
DSS		N/A
pCp-Cy3	Jena Bioscience	NU-1706-CY3
T7 RNA Polymerase	Thermo Fisher Scientific	AM2718
Phusion PCR kit	Thermo Fisher Scientific	F553L
Oligonucleotides		
siRNA	Millipore Sigma	NM_005548
Recombinant DNA		
HIV-1 RT (1-560)	ATUM (former DNA2.0)	N/A
pJexpress404	ATUM (former DNA2.0)	N/A
pET15b	Millipore Sigma	69661
Deposited Data		
Time dependence of the NMR spectra	This paper	https://doi.org/10.17632/zkc75shfc5.1
structure of HIV-1 RT (used)	Lansdon et al., 2010	PDB:3MEE
Software and Algorithms		
NMRPipe	IBBR/NIST	http://www.ibbr.umd.edu/nmrpipe/
NMRview	One Moon Scientific	http://onemoonsci.com/
ccpNMR	CCPN	http://www.ccpn.ac.uk/

LEAD CONTACT AND MATERIALS AVAILABILITY

Further information and requests for resources and reagents should be directed to and will be fulfilled by the Lead Contact, Rieko Ishima (ishima@pitt.edu).

EXPERIMENTAL MODEL AND SUBJECT DETAILS

Bacterial Strains

HIV-1 RT was expressed in commercially purchased *Escherichia coli* BL21(DE3) or Rosetta 2(DE3) cell lines.

Cells

We have used the reliable cell lines from AIDS reagent program (TZM-bl) or the American Type Culture Collection (HEK 293T). The 293T cell line is a highly transfectable derivative of human embryonic kidney 293 cells, and contains the SV40 T-antigen. TZM-bl is a HeLa cell line. Both cell lines tested negative for bacteria, mycoplasma and fungi.

Viruses

We have used HIV-1LAI which is an X4 tropic strain routinely used in *in vitro* HIV studies. All virus preparations were carried out in a Biosafety Level 2+ (BSL-2+) containment laboratory in accordance with proper BSL-2+ safety procedures.

METHOD DETAILS

In Vitro RT Maturation Experiments

RT proteins, p66/p51 and p66 alone were prepared using the p6HRT-PROT plasmid (Le Grice and Gruninger-Leitch, 1990), as described previously (Iliina et al., 2018). p66 protein was expressed in BL21 (DE3) *E. coli* cells and purified using a Strep-Trap HP column (GE Healthcare Lifesciences, Piscataway, NJ) and gel filtration on a Superdex 200 column (GE Healthcare, Piscataway, NJ). Purified proteins were stored in 25 mM sodium phosphate, pH 7.0, 250 mM NaCl and 50% v/v glycerol at -80°C. HIV-1 PR, clone purchased from ATUM (Newark, CA), was expressed and purified as described previously (Khan et al., 2018). Rilpivirine (RPV) and efavirenz (EFV) (Selleckchem, Houston, TX, and NIH AIDS reagent program) stock solutions, at 50 mM concentration, were prepared in 100% DMSO (Sharaf et al., 2016).

Proteolytic processing of p66 protein by HIV-1 PR was carried out in 20 mM sodium acetate buffer, pH 5.2, at 37°C. RPV was added to the reaction with a final DMSO concentration of 2%. All reactions that did not contain RPV included 2% DMSO for control. 4 μM of p66/p66, calculated as a dimer, was incubated for 5 min at room temperature in four conditions: p66 alone; with 4 μM tRNA^{Lys3}; with 4 μM RPV; with 4 μM tRNA^{Lys3} and 4 μM RPV. Processing was initiated by addition of HIV-1 PR to a final concentration 1 μM and incubated at 37°C. Aliquots were collected following different time intervals and quenched by the addition of Tricine sample loading buffer (Bio-Rad Laboratories, Berkeley, CA) and denatured at 95°C for 5 min. Samples were loaded onto precast 4-15% Tris-glycine gels (Bio-Rad), stained with Bio-safe Coomassie stain (Bio-Rad) and analyzed with Amersham Imager 600 (GE Healthcare Life Sciences).

In Vitro tRNA Transcription

tRNA^{Lys3} was prepared using a DNA template for tRNA transcription, which was PCR amplified using the following oligonucleotides as primers (Miller et al., 2004):

Coding strand: 5'-GCCCCGATAGCTCAGTCGGTAGAGCATCAGACTTTTAATCTGAGGGTCCA

GGGTTC AAGTCCCTGTTCCGGGCGCCA

Reverse primer: 5'-mUmGGCGCCCCGAACAGGGACTTG

Forward Primer: 5'- AATTCCTGCAGTAATACGACTCACTATAGCCCCGATAGCTCAGTCG.

PCR products were purified with phenol/chloroform extraction and used in transcription reactions. *In vitro* transcription of tRNA^{Lys3} was performed using NTPs and T7 RNA polymerase (Thermo Fisher Scientific, USA), as described by Sherlin et al. (Sherlin et al., 2001), and purified by anion exchange using Hi Trap Q HP column (GE Healthcare, Piscataway, NJ), desalted with PD-10 columns (GE Healthcare, Piscataway, NJ) and aliquoted for further use. Prior to each experiment tRNA was reannealed by heating at 95°C for 5 min followed by slow cooling to room temperature.

Analytical Size Exclusion Chromatography to Monitor p66/p66-tRNA Interaction

Size Exclusion Chromatography (SEC) experiments were performed using a 24-ml analytical Superdex 200 Increase 10/300 GL column (GE Healthcare), at room temperature at a flow rate of 0.5 mL/min. Either p66 protein at 20 – 46 μM, with 0 – 25 μM tRNA^{Lys3} or the tRNA^{Lys3} alone that contains tracer tRNA 3'-end labeled with pCp-Cy3 (Jena Bioscience, Jena, Germany) was prepared in 25 mM Bis-tris buffer, pH 7.0, containing 100 mM NaCl, 1% DMSO, and 0.02% sodium azide. RPV was added at [p66:p66]:[RPV] = 1: 1.3 or 1.5 ratio. Each injection volume was 50 μL. Elution profiles were monitored by UV absorbance at 254 and 280 nm and, for the samples with tRNA^{Lys3}, additionally by in-line Shimadzu RF-10AXL Fluorescence Detector with fluorescence excitation at 485 nm and the emission at 560 nm.

Sample Preparation for NMR Experiments

We used the same coding sequence of the RT p66 as described previously (Sharaf et al., 2014), except (i) a V559I polymorphism mutation was included to increase the number of Ile NMR resonances in ¹H-¹³C NMR spectra and (ii) an N-terminal His₆-fusion tag containing a TEV-protease cleavage site was added. [U-²H] and Ile ^δ¹-[¹³CH₃] labelled p66 and [U-²H, ¹⁵N] labelled p66 was

expressed using a published protocol (Tugarinov et al., 2006). In brief, isotopes were purchased from Cambridge Isotope Laboratories, Inc. (Tewksbury, MA) or MilliporeSigma (St. Louis, MO). Proteins were expressed in Rosetta 2(DE3) cells and were purified using HisTrap HP columns (GE Healthcare, Piscataway, NJ) and gel filtration on a Superdex 200 column (GE Healthcare, Piscataway, NJ). The N-terminal fusion tag was digested with His₆-TEV-protease. The p66 was separated from the remaining digestion products using a HisTrap HP column (GE Healthcare, Piscataway, NJ), followed by a final purification step on a Superdex 200 column (GE Healthcare, Piscataway, NJ). Purified proteins were exchanged to a buffer containing 50 mM Tris, 250 mM NaCl, 0.02% NaN₃ and 50% v/v Glycerol, pH 8.0 and stored at -80°C.

NMR Experiments

All the NMR experiments were recorded on a Bruker Avance 900 spectrometer. Prior to NMR, the buffers of all proteins were exchanged to a deuterated and non-deuterated, the latter containing 5% D₂O, 25 mM Bis-Tris buffer pH 7.1 containing 100 mM KCl, 0.02% NaN₃, and 5% v/v Glycerol-d₈ (named NMR buffer hereafter) for [U-²H] and Ile δ1-[¹³CH₃] labelled p66/p66, and for [U-²H,¹⁵N] labelled p66/p66, respectively. NMR experiments in the presence of RPV were performed by adding 0.5-1.0% d₆-DMSO in the NMR buffer.

The time-dependent spectral changes of 35 μM, [U-²H] and Ile δ1-[¹³CH₃] labelled p66/p66 were monitored by recording ¹H-¹³C SOFAST-HMQC spectra using Bruker sequence, sf_metrosygpqh, at time points 0, 4.85, 15.29, 20.12, 24.97, 29.80, 37.27, 42.42, 47.27, 52.10 and 56.95 hours at 35°C. The time point indicates the starting time of each HSQC spectrum which took 4.85 hours to complete. Because over 90% of p66 is expected to form a homodimer (Sharaf et al., 2014; Venezia et al., 2006), we simplify the expression as p66/p66, to complement the p66/p51 heterodimer description. The NMR spectra of the Ile δ1-labelled p66/p66 were compared to those of (1) p66/p51; and (2) of partially matured RT *in vitro*. For (1), p66/p51 protein was prepared by using [U-²H], Ile δ1-[¹³CH₃]-labelled p66 and unlabelled p51. Both p66/p66 and p66/p51 spectra were recorded using the NMR buffer, but without 100 mM KCl, at 35°C. For (2), partial maturation was achieved by adding 3 μM PR and ~20 μM tRNA^{Lys3} to the 25 μM [U-²H], Ile δ1-[¹³CH₃]-labelled p66/p66 solution in the NMR buffer, incubating at 35°C for 3 hours, followed by addition of the PR inhibitor, darunavir (obtained from NIH AIDS reagent program), to stop the reaction.

Spectral changes of p66/p66 upon interaction with tRNA^{Lys3} or RPV and with both tRNA^{Lys3} and RPV were monitored by recording ¹H-¹³C SOFAST-HMQC spectra of a ~25 μM [U-²H], Ile δ1-[¹³CH₃]-labelled p66/p66 in the deuterated NMR buffer at the anticipated ratios of tRNA^{Lys3}/[p66/p66] = 1.4, RPV/[p66/p66] = 2.0, and tRNA^{Lys3}/[p66/p66-RPV] = 1.0, at 35°C. Titrations of p66/p66 with RPV and with tRNA^{Lys3} in the presence of RPV were monitored by recording ¹H-¹³C SOFAST-HMQC spectra of the Ile δ1-labelled p66/p66, at 35°C, at relative concentrations of [RPV]:[p66/p66] of 0:1, 0.5:1, 1:1, and 2:1 and at [tRNA]:[p66/p66-RPV] of 0:1, 1:1, 2:1. These p66/p66 spectra, in the presence of tRNA^{Lys3}, RPV, or both, were also recorded at 20°C.

Spectral changes of p66/p66 upon interaction with these molecules were also monitored by recording ¹H-¹⁵N TROSY-HSQC spectra of 75 μM [U-²H, ¹⁵N]-labelled p66/p66 in the protonated NMR buffer at anticipated ratios of tRNA^{Lys3}/[p66/p66] = 1.0, RPV/[p66/p66] = 1.3, and tRNA^{Lys3}/[p66/p66-RPV] = 1.0, at 20°C. All the NMR spectra were processed using nmrPipe and analyzed using nmrDraw, nmrView or ccpNMR (Delaglio et al., 1995; Johnson, 2004; Vranken et al., 2005).

KARS Knockdown Experiments

Small interfering RNAs (siRNAs) targeting KARS, as well as a control scrambled sequence control siRNA, were purchased from Sigma (St Louis, MO, USA). 293T cells were transfected with 80-nmol/L siRNA using the Neon Transfection System (Thermo Fisher Scientific, USA), according to the manufacturer's protocol. The efficiency of gene knockdown was assessed by western blot analyses of protein expression. Anti-KARS antibodies were also purchased from Sigma. HEK 293T cells (ATCC® CRL-3216™) were transfected with HIV-1^{LAI} (Shi and Mellors, 1997) and RT and p24 antigen expression levels were measured by Western Blot (Abram and Parniak, 2005). Viral infectivity was assessed using TZM-bl cells (Giacobbi and Sluis-Cremer, 2017).

QUANTIFICATION AND STATISTICAL ANALYSIS

Figure 2: Bars show means ± S.D of intensity decay of 42 resonances picked by nmrDraw software.

Figure 5: Repeated experiment, repeated experiment using EFV, and experiments by varying RPV concentration are shown in Figures S1–S3.

Figure 6: Error bars in the graph were calculated from intensity uncertainty by nmrDraw software.

Figure 8: Bars show mean ± standard error from 3 independent experiments.

DATA AND CODE AVAILABILITY

All time dependence of the NMR spectra is available in Mendeley (<https://doi.org/10.17632/zkc75shfc5.1>).